LBL-28872
Preprint

Lawrence Berkeley Laboratory
UNIVERSITY OF CALIFORNIA

Materials & Chemical Sciences Division

Submitted to Journal of Chemical Physics

Photoelectron Spectroscopy and Electronic Structure of Clusters of the Group V Elements. II. Tetramers: Strong Jahn-Teller Coupling in the Tetrahedral ^2E Ground States of P_4^+, As_4^+ and Sb_4^+

L.-S. Wang, B. Niu, Y.T. Lee, D.A. Shirley,
E. Ghelichkhani, and E.R. Grant

June 1990

LOAN COPY
Circulates
for 2 weeks
Bldg. 50 Library.
LBL-28872
Copy 2

Prepared for the U.S. Department of Energy under Contract Number DE-AC03-76SF00098.

DISCLAIMER

This document was prepared as an account of work sponsored by the United States Government. While this document is believed to contain correct information, neither the United States Government nor any agency thereof, nor the Regents of the University of California, nor any of their employees, makes any warranty, express or implied, or assumes any legal responsibility for the accuracy, completeness, or usefulness of any information, apparatus, product, or process disclosed, or represents that its use would not infringe privately owned rights. Reference herein to any specific commercial product, process, or service by its trade name, trademark, manufacturer, or otherwise, does not necessarily constitute or imply its endorsement, recommendation, or favoring by the United States Government or any agency thereof, or the Regents of the University of California. The views and opinions of authors expressed herein do not necessarily state or reflect those of the United States Government or any agency thereof or the Regents of the University of California.

LBL-28872

Photoelectron Spectroscopy and Electronic Structure of Clusters of the Group V Elements. II. Tetramers: Strong Jahn-Teller Coupling in the Tetrahedral ^2E Ground States of P_4^+, As_4^+ and Sb_4^+

L.-S. Wang, B. Niu, Y.T. Lee, and D.A. Shirley
Department of Chemistry
University of California
and
Materials and Chemical Sciences Division
Lawrence Berkeley Laboratory
University of California
Berkeley, CA 94720

and

E. Ghelichkhani and E.R. Grant
Department of Chemistry
Purdue University
West Lafayette, IN 47907

This work was supported by the Director, Office of Energy Research, Office of Basic Energy Sciences, Chemical Sciences Division of the U.S. Department of Energy under Contract No. DE-AC03-76SF00098, by the National Science Foundation under Grant No. CHE-8920555, and by the Alexander von Humboldt Foundation through a Senior Scientist Award to DAS.

Abstract

High resolution HeI (584Å) photoelectron spectra have been obtained for the tetrameric clusters of the group V elements: P_4, As_4, and Sb_4. The spectra establish that the ground ^2E states of tetrahedral P_4^+, As_4^+, and Sb_4^+ are unstable with respect to distortion in the $\nu_2(e)$ vibrational coordinate. The $E \otimes e$ Jahn-Teller problem has been treated in detail, yielding simulated spectra to compare with experimental ones. Vibronic calculations, extended to second order (quadratic coupling) for P_4^+, account for vibrational structure which is partially resolved in its photoelectron spectrum. A Jahn-Teller stabilization energy of 0.65 eV is derived for P_4^+, which can be characterized in its ground vibronic state as being highly distorted, and highly fluxional. Linear-only Jahn-Teller coupling calculations performed for As_4^+ and Sb_4^+, show good qualitative agreement with experimental spectra, yielding stabilization energies of 0.84 eV and 1.4 eV, respectively.

I. Introduction

Elemental clusters fulfill a central role in contemporary chemistry as an important bridge between molecules and condensed matter. Increasingly, the focus of effort in cluster science is turning to questions concerned with the structural and dynamical properties of isolated clusters, and the relation of those properties to cluster reactivity.[1] This is a challenging problem, owing to the often complex vibrational and electronic structure of elemental clusters. Available spectroscopic methods fall short when applied to polydispersed clusters from supersonic expansions, and, outside of a few dimers and a handful of trimers, few data exist on the vibrational frequencies and electronic energy levels of neutral elemental clusters. The situation is a little better for charged clusters. For direct spectroscopy, size selection can be achieved by mass filtering, and information on the energy levels of neutral clusters can be obtained in transitions from negatively-charged clusters by photoelectron spectroscopy, with accompanying confirmation of parent mass.[2] Much of this work has focussed on transition metals. Main group elements also form interesting and important clusters. In particular, the elements of Group V have long been known to form molecularly bound clusters, especially tetrahedral tetramers.[3] We have exploited the naturally high concentration of such species in supersonic expansions of the Group V elements from a high temperature molecular beam source to obtain structural details on the geometries and energy levels of the corresponding cations. In part I of our investigation,[4] we reported on the high resolution photoelectron spectroscopy of the dimers: As_2, Sb_2, and Bi_2. In the current paper, we turn our attention to the tetrameric systems: P_4, As_4, and Sb_4.

Among the polyatomic clusters, only Cu_3,[5] Na_3,[6] and Li_3,[7] have thus far been spectroscopically well characterized. Interestingly, spectroscopic data for all of these trimers establish that Jahn-Teller effects play an important role in determining their ground state properties. In each case, the trimers in D_{3h} symmetry have a ^2E ground state, which

couples with the doubly degenerate $\nu_2(e)$ vibrational mode. Symmetric geometries are envisioned for higher clusters, and Jahn-Teller effect may well extend to such systems.

The tetramers of P, As, and Sb have T_d symmetry with a $^1A_1$ ground state. In T_d symmetry, molecular orbital calculations show that the ground state term of the tetrameric cations is ^2E, while that of their first excited states is $^2T_2$.[8] Both these states, being orbitally degenerate, are subject to Jahn-Teller distortions. Thus, these species can be viewed as prototypes for studying the Jahn-Teller effect in larger metal clusters with T_d symmetry.

Lower resolution HeI photoelectron spectra of P_4,[9] As_4,[10] and Sb_4[11,12] have been reported. Except for the $^2A_1$ state of P_4^+, no vibrational resolution has been achieved. Hence, little is known about the spectroscopy of the cationic states of these simple cluster species. A few electronic structure calculations exist for the neutral clusters, P_4,[8,13] As_4,[13a,14] and Sb_4.[12] But as yet none have been carried out for the ionic states.

We have obtained high resolution photoelectron spectra for all three cluster species. Vibrational structure is completely resolved for the $^2A_1$ states of P_4^+ and As_4^+, while that in the Jahn-Teller active ^2E and $^2T_2$ states is only partially resolved due to smaller vibrational frequencies. Strong Jahn-Teller distortions are found in the ^2E states, owing to coupling in the ν_2 vibrational coordinate, in each case splitting the spectra into two broad bands. In the current paper, we focus on the ground ^2E states. The $E\otimes e$ Jahn-Teller problem is explored in detail for the ^2E states of these tetrameric cations, representing the first vibronic studies for T_d clusters. The $^2T_2$ and $^2A_1$ states will be discussed in a subsequent paper.

The rest of the paper is organized as follows. In Section II, we briefly present the experimental procedure. The results are presented in Section III. The discussion and the comparisons of the vibronic calculations with the experimental results are given in Section IV. The conclusions appear in Section V.

II. Experimental

The high temperature molecular beam source used in the current experiments has been described in detail previously.[15] The experimental conditions related to the current experiments are given collectively in Table 1. As pointed out previously,[3,4] evaporations of pure phosphorus and arsenic give essentially neat tetramer species. Pure elements are used for all three cases. Phosphorus has three allotropic forms, white, red, and black. The white form is highly reactive even at room temperature and difficult to handle.[3] So, the more stable red form is used. Antimony is less volatile, and a higher temperature is required for the experiment. At the experimental temperature given in Table 1, the vapor of antimony contains three species: atoms, dimers, and tetramers. As a result, the photoelectron spectrum is a mixture of the three. The bismuth vapor is composed of both atoms and dimers, but the atomic contributions to the photoelectron spectrum can be easily subtracted, and a pure dimer spectrum can be still obtained. All samples (99% purity) were purchased from CERAC and used directly.

The details of the photoelectron spectrometer have also been described previously.[16] Argon and xenon are used as calibration gases. The energy resolution is 12 meV, as measured with the Ar^+ $^2P_{3/2}$ photoelectron peak. To avoid drift of the energy scale under high temperature conditions, we have kept each photoelectron scan under one hour. Multiple scans have been taken and added together to increase counting statistics. The effective energy resolution on the final spectrum is about 15 meV.

III. Results

The photoelectron spectra of P_4, As_4, and Sb_4 are shown in Figures 1-3, respectively. The three clusters are isoelectronic and all have the same tetrahedral geometry. Thus, their photoelectron spectra are very similar, with the P_4^+ and As_4^+ spectra showing vibrational resolution. Under T_d symmetry, the valence electronic configuration of these clusters can be written as:

$$(1a_1)^2\,(1t_2)^6\,(2a_1)^2\,(2t_2)^6\,(1e)^4$$

where the $1a_1$ and $1t_2$ MOs are mainly of the valence atomic s orbital character, and the $2a_1$, $2t_2$, and 1e MOs of the valence p character. As pointed out previously,[4] the atomic ionization cross sections of the ns orbitals are two to three orders of magnitude smaller than the np orbitals at the HeI photon energy (21.218).[17] Consequently, the $1a_1$ and $1t_2$ MOs also have very small ionization cross sections. Thus, only the ionizations of the outermost three MOs are observed, as indicated in Figures 1-3. The Sb_4^+ spectrum has a contribution from the Sb_2 species, as noted in Figure 3. The $^2\Pi_u$ bands of Sb_2^+ overlap exactly with the $(2t_2)^{-1}$ bands of Sb_4^+, though the contribution from the $^2\Pi_u$ bands of Sb_2^+ is expected to be small. Both the small vibrational frequencies and the poor statistics in the Sb_4^+ spectrum are responsible for the lack of vibrational structure, particularly in the $(2a_1)^{-1}$ band.

With T_d symmetry, these three clusters have $^1A_1$ ground states. Removal of an electron from the 1e or $2t_2$ MOs creates ^2E and $^2T_2$ final states in the ions, respectively. The ^2E state is orbitally doubly degenerate and the $^2T_2$ state triply degenerate. According to the Jahn-Teller theorem,[18] these two states are Jahn-Teller active and the tetrahedral geometries of the molecular ions are unstable in these two states against asymmetric vibrations. The $^2A_1$ excited states of the molecular ions from $(2a_1)^{-1}$ are not orbitally degenerate and should maintain the T_d symmetry.

The six normal modes of vibrations for a tetrahedral M_4 molecule are shown in Figure 4. The ν_2 (e) mode is doubly degenerate and the ν_3 (t_2) mode is triply degenerate. The vibrational frequencies for P_4, As_4, and Sb_4 are given in Table 2. The ν_1 (a) mode is totally symmetric and cannot distort the T_d symmetry. However, the ν_2 and ν_3 modes are both Jahn-Teller active. From group theory, only the ν_2 mode can be Jahn-Teller active in the ^2E state while both the ν_2 and ν_3 modes can be coupled in the $^2T_2$ state.[19] In the present paper, we focus on a full analysis of the vibronic structure observed in each case for the ^2E cation ground states. In the following paper, we consider more qualitative aspects of the structure of excited state bands, as well as overall trends in ionization potential.

It can be seen from Figures 1-3 that two photoelectron bands are observed for ionization of the 1e orbital as a result of the Jahn-Teller coupling with the ν_2 vibrations (see below). Because of the strong Jahn-Teller effect, adiabatic IPs to the ground ^2E states can not be obtained by direct inspection, and only upper limits can be estimated from the experimental photoelectron spectra. Vibronic calculations yield better values for the adiabatic IPs.

IV. Discussion: The Jahn-Teller Effect and Vibronic Structure in the ^2E Ground States of T_d Group V Cation Tetramers

A. Potential Energy Surfaces

The prominent two-peaked spectral intensity distributions evident to a remarkable similar degree in the $(1e)^{-1}$ bands of all three tetramers signal strong Jahn-Teller distortions differentiating the molecular ion ground states from the highly symmetric tetrahedral configurations of the corresponding neutrals. As noted above, the ^2E ($G_{3/2}$) terms associated with these 1e-orbital vacancies are, in each case, subject to Jahn-Teller vibronic coupling in the ν_2(e) normal coordinate. This coupling displaces stable molecular

configurations from high symmetry, and, as a consequence, distributes spectral intensity over progressions of vibronically excited bands. A qualitative understanding of this effect can be achieved by examining the adiabatic potential energy surfaces of the Jahn-Teller active system in classical terms.

Let $\psi_\pm$ denote the complex electronic wave functions of the doubly degenerate electronic term, and $H_e(Q_0)$ the electronic Hamiltonian at the undistorted nuclear configuration. Surfaces of the single-mode E⊗e Jahn-Teller problem are obtained most simply by diagonalizing the electronic Hamiltonian in a diabatic basis that spans the symmetry-induced two-fold electronic degeneracy:[20]

$$\begin{bmatrix} \langle\psi_+|H_e(Q_0)|\psi_+\rangle - E(Q) & \langle\psi_+|H_e(Q_0)|\psi_-\rangle \\ \langle\psi_-|H_e(Q_0)|\psi_+\rangle & \langle\psi_-|H_e(Q_0)|\psi_-\rangle - E(Q) \end{bmatrix} \begin{bmatrix} a(Q) \\ b(Q) \end{bmatrix} = 0 \ , \tag{1}$$

in which, as indicated explicitly below, single-term harmonic expansions conventionally approximate diagonal matrix elements, while linear terms lead expansions of off-diagonal elements.[21] Eq.(1) is the quantum mechanical starting point to discuss the Jahn-Teller coupling between a doubly degenerate electronic state and a doubly degenerate vibrational mode. The resulting surfaces, E(Q), show, in lowest order, linear divergence from the symmetric point, characteristic of a conical intersection, which, when combined with a harmonic restoring force, produces the familiar cylindrically symmetric sombrero double-valued potential, described by the equation:

$$E_\pm(Q) = \frac{1}{2}\rho^2 \pm k\rho \ , \tag{2}$$

where k is the linear coupling coefficient expressed in units for which λ, the harmonic force constant, equals one. Figure 5 illustrates this simplest Jahn-Teller potential surface.

The level structure and vibrational dynamics associated with such potentials are generally more complex, characterized by spectral irregularity and the facile exchange of

angular momentum between vibrational and electronic subsystems.[22-24] However, for low-lying levels carried far from the conical intersection by strong linear coupling, a simple adiabatic separation can provide an intuitively appealing picture, which accounts for evident patterns of transitions by mapping observed structure on the model of a radial oscillator combined with a free internal rotor moving on the lower sheet. The quantum states of this limit are approximately described by the simple expression:[25]

$$W(n,j) = nh\omega + Aj^2 \tag{3}$$

in which ω is the characteristic frequency, n is the quantum number of the radial oscillator, and A is an internal rotation constant:

$$A = \frac{h^2}{2M\rho_0} \tag{4}$$

where M is the reduced mass of the mode and ρ_0 is the radial minimum on the lower surface. j is the vibrational angular momentum quantum number, constrained to be half-odd integral by boundary conditions imposed by topological phase.[26]

The simple picture of a system of transitions from the ground state of the neutral to vibrational levels of the cylindrically distorted adiabatic lower surface accounts well for the long progressions of the bands that characterize the first broad peaks of the spectra of P_4^+, As_4^+, and Sb_4^+. Similarly extending an adiabatic separation to the upper surface, we can calculate a harmonic set of widely spaced eigenstates of the steeper upper potential. In reality, these are, of course, imbedded in the dense manifold of states of the lower sheet, to which they are coupled by nonadiabatic terms. However, as discussed below, in exact nonadiabatic calculations based on the lower-order Hamiltonian, they survive as quasi-resonances,[27] which have been recognized in theory as useful semiclassical markers of coupling strength.[28] Thus, we can associate the second broad maximum in the

photoelectron spectra with a concentration of Franck-Condon intensity about the origin of the upper sheet, and predict additional maxima at intervals of higher energy.

Though the properties of such cone resonances, and the coupling conditions under which they can be expected to appear, are well characterized theoretically,[27-29] no experimental examples exist that show oscillatory behavior beyond the broad bifurcation also evident in the photoelectron spectra. This may be a question of resolution; conventional photoelectron spectroscopy resolves well electronic separations, but tends to smear structure on the scale of vibrational progressions, particularly for heavier, lower-frequency systems. The spectra presented in Figures 1-3 offer a higher resolution view of what are evidently strongly coupled systems. It is thus worthwhile to compare these spectra with theory at the highest feasible level of exact calculation in an effort to refine our semiclassical understanding of higher-lying quantum states in realistic strongly-coupled systems.

B. Exact Nonadiabatic Calculations

Retaining the form of the Hamiltonian (1), which assumes a well-isolated degenerate electronic term, and further assuming the adequacy of a harmonic basis to describe motion in Q, we can write the Schrodinger equation to second order in vibrational amplitude, ρ, and phase, ϕ:

$$\left[T_N \mathbf{1} + \begin{bmatrix} \frac{\rho^2}{2} & k\rho e^{-i\phi} + \frac{g\rho^2 e^{2i\phi}}{2} \\ k\rho e^{i\phi} + \frac{g\rho^2 e^{-2i\phi}}{2} & \frac{\rho^2}{2} \end{bmatrix} \right] \begin{bmatrix} \chi_+ \\ \chi_- \end{bmatrix} = W \begin{bmatrix} \chi_+ \\ \chi_- \end{bmatrix} , \qquad (5)$$

in which nuclear kinetic energy T_N is diagonal, and coefficients k and g characterize linear and quadratic distortion terms, in units of the harmonic restoring force. We expand χ_+ and χ_- in a basis of isotropic harmonic oscillator wave functions:

$$\chi_+ = \sum a_{\nu,l} |\nu,l\rangle \tag{6}$$

$$\chi_- = \sum b_{\nu,l} |\nu,l\rangle \tag{7}$$

$$\nu = 0, 1, 2, \ldots \tag{8}$$

$$l = -\nu, -\nu+2, \ldots, \nu-2, \nu \tag{9}$$

where the oscillator frequency is chosen so that $|\nu,l\rangle$ are eigenfunctions of the diagonal vibrational Hamiltonian. The explicit form of the expanded matrix is simplified by recognizing that the polar normal coordinates, $\rho e^{-i\phi}$ and $\rho e^{i\phi}$, function as raising and lowering operators with respect to the l vibrational angular momentum quantum number, viz:

$$\langle \nu, l\, | \rho e^{-i\phi} | \nu+1, l+1 \rangle = \sqrt{\frac{(\nu+l+1)}{2}}\ , \tag{10}$$

$$\langle \nu-1, l\, | \rho e^{i\phi} | \nu, l \rangle = \sqrt{\frac{(\nu-l-1)}{2}} \tag{11}$$

and, with

$$\langle \nu, l\, | \rho^2 e^{-2i\phi} | \nu', l' \rangle = \sum_{\nu'',l''} \langle \nu, l\, | \rho e^{-i\phi} | \nu'', l'' \rangle \langle \nu'', l''\, | \rho e^{-i\phi} | \nu', l' \rangle \tag{12}$$

we construct non-zero matrix elements of the quadratic terms:

$$\langle \nu, l\, | \rho^2 e^{-2i\phi} | \nu, l+2 \rangle = \sqrt{(\nu+l+1)(\nu-l-1)} \tag{13}$$

$$\langle \nu, l\, | \rho^2 e^{-2i\phi} | \nu+2, l+2 \rangle = \frac{\sqrt{(\nu+l+1)(\nu+l+3)}}{2} \tag{14}$$

$$\langle \nu, l \,|\rho^2 e^{-2i\phi}|\nu\text{-}2, l\text{+}2\rangle = \frac{\sqrt{(\nu\text{-}l\text{-}1)(\nu\text{-}l\text{-}3)}}{2} \tag{15}$$

The resulting sparse matrix is diagonalized to obtain level energies and spectral overlaps.

C. Distortion and Hindered Fluxionality in the Ground State of P_4^+

The vibronic spectrum of the conical intersection is particularly simple for the case in which it is assumed that g = 0. The problem then block-factors according to the quantum number j, corresponding to the half-odd integral vibrational angular momentum, and only blocks with $j = \pm\frac{1}{2}$ carry transition intensity. Under such conditions, fully converged calculations can be extended over a large range of energy using conventionally available diagonalization subroutines. Figure 6 shows a correlation diagram giving the relative energies of the first few excited states of the linearly coupled Hamiltonian as a function of the stabilization energy, $D = \frac{1}{2}k^2$, from D = 0 to the adiabatically separable limit. Figure 7 compares theoretical positions and intensities with experimental results for P_4^+, for a model that assumes single-mode linear coupling with k = 5.75 in units of the zeroth-order frequency, which is taken to be 315 cm^{-1}, the experimentally observed vibrational spacing. It can be seen that the theory and experiment agree very well, particularly in the qualitative shape of the first broad maximum and the leading edge of the second band. The fit of the theoretical envelope to the experimental one yields an improved estimate of the adiabatic ionization threshold, 8.95 eV, which is difficult to obtain from the experimental photoelectron spectrum. With reference to Figure 5, the Jahn-Teller stabilization energy of P_4^+ in this simple linear model is 0.65 eV, which places the conical intersection at an ionization potential of 9.60 eV, and fully 15 levels of radial oscillation between the zero point and the beginning of the upper sheet. Theoretical intensities show a slight modulation in the upper range of the spectral envelope associated with the cone-resonances

phenomenon noted above. Experimental limitations imposed by resolution together with the proximity of the $(2t_2)^{-1}$ transition prevent the confirmation of such structure in the data, though the bandshape observed certainly does not rule out this intensity pattern.

The question of the subtle pattern of intensities and the degree to which they match the predictions of the simple linear model is one of qualitative importance. If a system such as P_4^+ is accurately described by a Hamiltonian coupled strictly to first order in the distortion coordinates, it then follows that the potential in these coordinates is cylindrically symmetric, presenting no barrier to vibronic pseudorotation. Under such circumstances, we must characterize the system not only as strongly distorted, but highly fluxional as well. If, on the other hand, theory requires higher-order coupling terms to account for spectral positions and intensities, we must then recognize potential barriers that quench free rotation in the phase of the distortion for the lowest radial levels.

Diagonalizing the electronic part of the problem as in (1) for the explicit matrix elements expressed in the linear-plus-quadratic Hamiltonian (5) yields a more complex adiabatic potential:

$$E_{\pm}(\rho,\phi) = \tfrac{1}{2}\rho^2 \pm k\rho\left[1 + \frac{g\rho}{k}\cos(3\phi) + \frac{g^2\rho^2}{4k^2}\right]^{1/2} \tag{16}$$

For small g/k, this expression simplifies to read:

$$E_{\pm}(\rho,\phi) = \frac{1}{2}\left[\rho^2 \pm g\rho^2\cos(3\phi)\right] \pm k\rho \tag{17}$$

using (17) to identify maxima and minima in the floor of the lower sheet, we can solve for the pseudorotation barrier as a function of k and g:

$$E(\rho_0,\phi_{max/min}) = -\frac{k^2}{2(1\pm g)} \tag{18}$$

The matrix elements that produce these modulations couple vibrational basis states in a scheme that block-factors as j' = j mod 3. As a result, with reference to the correlation diagram in Figure 6, accidentally degenerate eigenstates of the linear-only Hamiltonian with $j = \pm\frac{3}{2}, \frac{9}{2}, \frac{15}{2}, \ldots$ split, and other levels, which are closely lying in the linear approximation and belong to the same j' block, similarly diverge and share intensity. Figure 8 illustrates the effect of including quadratic coupling on the simulated spectrum of P_4^+, retaining the linear parameter of Figure 7. As can be seen, by distributing the oscillator strength of the radial fundamentals over all the added states of the $j = \pm\frac{1}{2}$ mod 3 block, higher-order coupling greatly increases the density of allowed transitions. Interestingly, however, broader intensity patterns are less affected, and when simulated spectra are convoluted with a 15 meV instrumental function, the overall bandshape remains roughly constant over the full range of quadratic coupling for which we can obtain converged intensities.

However, one important trend can be recognized. For g = 0, the family of transitions to the $j = \frac{1}{2}$ radial fundamentals form a highly regular progression of bands. The addition of quadratic barriers of a magnitude comparable to the zero-point energy initially disrupts this structure, spreading intensity over an irregular distribution of states, and thus smoothing the leading edge of the first band for values of g that fall in the range from 0.005 to 0.02. For g greater than 0.02 quadratic pseudorotation barriers significantly exceed the radial vibrational frequency. These larger modulations of the pseudorotation moat trap lower-lying vibrational states in three-fold wells. The associated vibrational structure tends toward that of statically distorted isomers, with an increased periodicity, broken by tunneling splitting and above-barrier reflection. As a result, we recognize that lower and higher extremes of quadratic coupling are spectroscopically characterized by periodic intensity modulations. The P_4^+ spectrum displays sufficient resolution to show periodic structure on the trailing edge of the first band. But, the leading edge of this band is comparatively smooth. Such behavior is encompassed by only a relatively narrow range of quadratic coupling coefficients, including g from about 0.01 to 0.02.

Thus, we have a quantitative picture of the Jahn-Teller coupling in the ^2E state of P_4^+ that is reasonably secure to second order. The largest term coupling the electronic degeneracy is linear in the e vibrational coordinate, producing a strong distortion, stabilized by 0.65 eV relative to the symmetric configuration. The resulting vibronic pseudorotation trough is modulated by a moderate higher-order coupling, which erects a three-fold barrier with a height comparable to the zero-point energy. A potential energy surface illustrating the relative magnitude of these effects is presented in Figure 9. The principal observable consequence of the dominant linear distortion is the transfer of Franck-Condon intensity to transitions that produce vibronically excited ions, which form a spectrum with a distinctive double maximum. By quenching vibronic angular momentum, quadratic coupling widens this intensity distribution to include transitions forbidden under conditions of linear coupling alone, which, at the level appropriate to explain the P_4^+ spectrum, smooths the leading edge of the first band.

D. Strong Vibronic Couplings in As_4^+ and Sb_4^+: The Cases for Cone Resonances in Realistic Systems

The qualitative features of the $(1e)^{-1}$ bands of As_4^+ and Sb_4^+ are similar to that of P_4^+ and can be interpreted similarly. However, it is more difficult to be as precise in our vibronic assessments of As_4^+ and Sb_4^+. Neither spectrum exhibits discernable structure that can be associated with individual vibrational bands. Nevertheless, the neutral ground state frequencies are known,[30] and a simple linear approach can be used just as with P_4^+ to characterize the gross properties of vibronic distortions responsible for the observed photoelectron spectra. Figures 10 and 11 show our spectral simulations for linear coupling parameters of k = 9.5 and 12.5, respectively. The spectral envelopes obtained from these linear-only simulations correspond with experimental ones quite well, even though it appears very likely that a complete description will require some degree of higher-order coupling: leading linear terms are larger for As_4^+ and Sb_4^+ than for P_4^+, and spectral

intensity is sufficiently redistributed to obscure discrete band structure. Most interesting is the absence in the experimental spectra of continuing intensity oscillations beyond the first. These oscillations are the exact manifestations in linearly coupled calculations of the semiclassical cone resonances discussed above. The linear coupling terms for the cases at hand are too large, and the energies that need to be considered too high, to extend calculations to the dimensions required for the addition of quadratic terms, so we cannot test the persistence of these features at higher orders of theory. We suspect that they will be moderate, and that their absence in the present spectra can be explained by a realistic order of coupling, with attendant mixing and disruption of cone resonances.

By analogy with P_4^+, linearly-coupled spectral simulations suffice to broadly characterize vibronic distortion in these systems. Taken together, the resulting coupling parameters establish obvious trends in the potential energy surfaces and vibronic state distributions for the $(1e)^{-1}$ band of the group V tetramer cations. As noted above, correspondence between experiment and theory places the adiabatic IP of P_4 at 8.95 eV, with about 15 radial vibronic energy levels between the distorted zero point of the cation and its symmetric conical intersection 0.65 eV higher. In As_4^+ and Sb_4^+, distortions are successively deeper. The adiabatic IP of As_4, established by linear simulation to be 7.83 eV, lies 0.84 eV below the energy of the cationic conical intersection. For Sb_4^+, we estimate an adiabatic threshold of 6.61 eV, stabilized 1.4 eV by the Jahn-Teller distortion. Adding to the impact of these moderately deepening distortions is the effect of diminishing vibrational frequency. Because the associated frequencies are so much smaller, the potential surfaces of the heavier systems contain many more adiabatically separable vibronic states; respective pseudorotation troughs support about 45 overtones of the radial oscillation for As_4^+, and nearly 80 for Sb_4^+.

The derived adiabatic ionization potentials and the Jahn-Teller stabilization energies for the three cluster ions are summarized in Table 3.

V. Conclusions

First photoelectron bands P_4^+, As_4^+, and Sb_4^+ have been analyzed in detail in terms of the vibronic consequences of E⊗e Jahn-Teller coupling. For P_4^+, spectral simulations for linear coupling with a constant of k=5.75 agree well with experiment. Refinement in terms of higher order coupling terms improves the agreement between theory and experiment. Best fits add small quadratic terms to the same linear distortion, predicting quadratic barriers to pseudorotation comparable to the zero-point energy. Thus, P_4^+ is characterized in its ground vibronic state as both highly distorted and highly fluxional. Cone-resonances appear in the calculated spectra, but appear disrupted by higher-order coupling in real systems. Linear-only calculations on As_4^+ and Sb_4^+ also agree well with the experiment, though the effects of higher order couplings remain evident. Quantitative account of vibronic coupling is essential for accurate estimate of adiabatic ionization potentials.

Acknowledgment

DAS thanks the Alexander von Humboldt Foundation for support through a Senior Scientist Award, and Professors G. Kaindl and E. Mattias for their hospitality during his stay in FB Physik, FU Berlin. Theoretical contributions by EG and ERG have been supported by the National Science Foundation under Grant No. CHE-8920555. The experimental work was supported by the Director, Office of Energy Research, Office of Basic Energy Sciences, Chemical Sciences Division of the U.S. Department of Energy under Contract No. DE-AC03-76SF00098.

References

1. (a) A. Kaldor, D. Cox, and M.R. Zakin, *Ad. Chem. Phys.* **70**, 211 (1988); (b) R.L. Whetten and K.E. Schriver, in *Gas Phase Inorg. Chem.*, D.H. Russell, Ed., (Plenum, New York, 1989), p193; (c) D.J. Trevor, D. Cox, and A. Kaldor, *J. Am. Chem. Soc.* **112**, 3742 (1990); (d) Lihong Wang, C.P.F Chibante, F.K. Tittel, R.F. Curl, and R.E. Smalley, *J. Am. Chem. Soc.*, to be published.
2. (a) O. Cheshnovsky, K.J. Taylor, J. Conceicao, and R.E. Smalley, *Phys. Rev. Lett.* **64**, 1785 (1990); (b) K.M. Ervin, J. Ho, and W.C. Lineberger, *J. Chem. Phys.* **89**, 4514 (1988).
3. A.N. Nesmeyanov, R. Gary (ed.), *Vapor Pressure of the Chemical Elements* (Elsevier, Amsterdam, 1957).
4. L.S. Wang, Y.T. Lee, D.A. Shirley, K. Balasubramanian, and P. Feng, Part I, (in preparation).
5. (a) D.P. DiLella, K.V. Taylor, and M. Moskovits, *J. Phys. Chem.* **87**, 524 (1983); (b) M.D. Morse, J.B. Hopkins, P.R.R. Langridge-Smith, and R.E. Smalley, *J. Chem. Phys.* **79**, 5316 (1983); (c) T.C. Thompson, D.G. Truhlar, and C.A. Mead, *J. Chem. Phys.* **82**, 2392 (1985); (d) W.H. Crumley, J.S. Hayden, and J.L. Gole, *J. Chem. Phys.* **84**, 5250 (1986).
6. (a) A. Herrmann, M. Hofmann, S. Leutwyler, E. Schumacher, and L. Woste, *Chem. Phys. Lett.* **62**, 216 (1979); (b) J.L. Gole, G.J. Green, S.A. Pace, and D.R. Preuss, *J. Chem. Phys.* **76**, 2247 (1982); (c) S.C. Ritchtsmeler, M.L. Hendewerk, D.A. Dixon, and J.L. Gole, *J. Phys. Chem.*, **86**, 3932 (1982); (d) M. Broyer, G. Delacretaz, P. Labastie, J.P.Wolf, and L. Woste, *Phys. Rev. Lett.* **57**, 1851 (1986); (e) M. Broyer, G. Delacretaz, G.Q. Ni, R.L. Whetten, J.P. Wolf, and L. Woste, *Phys. Rev. Lett.*, **62**, 2100 (1989).

7. (a) W.H. Gerber and E. Schumacher, *J. Chem. Phys.* **69**, 1692 (1978); (b) J.L. Gole, R.H. Childs, D.A. Dixon, and R.A. Eades, *J. Chem. Phys.* **72**, 6368 (1980); (c) R.A. Eades, M.L. Hendewerk, R. Frey, D.A. Dixon, and J.L. Gole, *J. Chem. Phys.* **76**, 3075 (1982); (d) J.L. Martins, R. Car, and J. Buttet, *J. Chem. Phys.* **78**, 5646 (1983); (e) T.C. Thompson, G. Izmirlian, Jr., S.J. Lemon, D.G. Truhlar, and C. A. Mead, *J. Chem. Phys.* **82**, 5597 (1985); (f) J.D. Wolf, G. Delacretaz, and L. Woste, *Phys. Rev. Lett.* **63**, 1946 (1989).

8. M.F. Guest, I.H. Hillier, and V.R. Saunders, *J. Chem. Soc. Faraday Trans* II **68**, 2070 (1972).

9. (a) S. Evans, P.J. Joachim, A.F. Orchard, and D.W. Turner, *Int. J. Mass Spectrom. Ion Phys.* **9**, 41 (1972); (b) C.R. Brundle, N.A. Kuebler, M.B. Robin, and H. Basch, *Inorg. Chem.* **11**, 20 (1972); (c) H. Bock and H. Muller, *Inorg. Chem.* **23**, 4365 (1984).

10. (a) S. Elbel, H.T. Dieck, H. Walther, and J. Krizek, *Inorg. Chim. Acta* **53**, L101 (1981); (b) J.M. Dyke, S. Elbel, A. Morris, and J.C.H. Stevens, *J. Chem. Soc. Faraday Trans.* II **82**, 637 (1986).

11. J.M. Dyke, A. Morris, and J.C.H. Stevens, *Chem. Phys.* **102**, 29 (1986).

12. S. Elbel, J. Kudnig, M. Grodzicki, and H.J. Lempka, *Chem. Phys. Lett.* **109**, 312 (1984).

13. (a) G. Trinquier, J.P. Malrieu, and J.P. Daudey, *Chem. Phys. Lett.* **80**, 552 (1981); (b) U. Wedig, H. Stoll, and H. Preuss, *Chem. Phys.* **61**, 117 (1981); (c) K. Raghavachari, R.C. Haddon, and J.S. Binkley, *Chem. Phys. Lett.* **122**, 219 (1985).

14. J. Andzelm, N. Russo, and D.R. Salahub, *Chem. Phys. Lett.* **142**, 169 (1987).

15. (a) L.S. Wang, B. Niu, Y.T. Lee, and D.A. Shirley, *Chem. Phys. Lett.* **158**, 297 (1989); (b) L.S. Wang, B. Niu, Y.T. Lee, D.A. Shirley, and K. Balasubramanian, *J. Chem. Phys.* **92**, 899 (1990); L.S. Wang, J.E. Reutt-Robey, B. Niu, Y.T. Lee, and D.A. Shirley, J. *Electron Spectrosc. Relat. Phenom.* **51**, 513 (1990).

16. J.E. Pollard, D.J. Trevor, Y.T. Lee, and D.A. Shirley, *Rev. Sci. Instrum.* **52**, 1837 (1981).

17. J.J. Yeh and I. Lindau, *Atomic Data and Nuclear Data Tables* **32**, 1 (1985).

18. H.A. Jahn and E. Teller, *Proc. Roy. Soc.* **A161**, 220 (1937).

19. G. Herzberg, *Molecular Spectra and Molecular Structure III. Electronic Spectra and Electronic Structure of Polyatomic Molecules* (Van Nostrand Reinhold, New York, 1966).

20. (a) A.D. Liehr, *Ann. Rev. Phys. Chem.* **13**, 41 (1962); (b) A.D. Liehr, *J. phys. Chem.* **67**, 389 & 471 (1963).

21. H.C. Lonquet-Higgins, *Adv. Spectrosc.* **2**, 429 (1961).

22. R.L. Whetten, G.S. Ezra, and E.R. Grant, *Ann. Rev. Phys. Chem.* **36**, 277 (1985).

23. (a) H. Koppel, L.S. Cederbaum, W. Domcke, and S.S. Shaik, *Ang. Chem. Int. Ed.* **22**, 210 (1983); (b) H. Koppel, W. Domcke, and L.S. Cederbaum, *Adv. Chem. Phys.* **57**, 59 (1984).

24. (a) J.W. Zwanziger, E.R. Grant, and G.S. Ezra, *J. Chem. Phys.* **85**, 2089 (1986); (b) J. W. Zwanziger and E.R. Grant, *J. Chem. Phys.* **90**, 2357 (1989).

25. H.C. Lonquet-Higgins, U. Opik, M.H.L. Pryce, and R.A. Sack, *Proc. Roy. Soc. London Ser. A* **244**, 1 (1958).

26. J.W. Zwanziger and E.R. Grant, *J. Chem. Phys.* **87**, 2954 (1987).

27. T.C. Thompson, D.G. Truhlar, and C.A. Mead, *J. Chem. Phys.* **82**, 2302 (1985).

28. H. Koppel, E. Haller, L.S. Cederbaum, and W. Domcke, *Mol. Phys.* **41**, 669 (1980).

29. R.L. Whetten, K.S. Haber, and E.R. Grant, *J. Chem. Phys.* **84**, 1270 (1986).

30. (a) S.B. Brumbach and G.M. Rosenblatt, *J. Chem. Phys.* **56**, 3110 (1972); (b) V.E. Bondybey, G.P Schwartz, and J.E. Griffiths, *J. Mol. Spectrosc.* **89**, 328 (1981).

31. H.S. Gutowsky and L.T. Hoffman, *J. Am. Chem. Soc.* **72**, 5751 (1950).

32. D.R. Pooler, in *The Dynamical Jahn-Teller Effect in Localized Systems*, Yu. E. Perlin and M. Wagner, eds. (Elsevier, New York, 1984).

Table 1. Experimental conditions.

	T (K)[a]	P (Torr)[b]	ϕ (mm)[c]	Starting materials[d]
P_4	620	500 (He)	0.16	Pure red phosphorus
As_4	650	200 (He)	0.16	Pure arsenic
Sb_4	1150	600 (Ne)	0.13	Pure antimony

a. Oven temperature (±50 K).

b. Carrier gas pressure.

c. Nozzle diameter.

d. Samples purchased from CERAC.

Table 2. Ground state vibrational frequencies (cm^{-1}) of P_4, As_4, and Sb_4.

	P_4[a]	As_4[b]	Sb_4[c]
$\nu_1(a_1)$	606	344	241
$\nu_2(e)$	363	210	140
$\nu_3(t_2)$	464.5	255	179

a. From Ref. 31.

b. From Ref. 30(a).

c. From Ref. 30(b).

Table 3. Estimated adiabatic ionization potentials (IPa) and Jahn-Teller stabilization energies (D) for the $(1e)^{-1}$ bands of P_4^+, As_4^+, and Sb_4^+.

	P_4^+	As_4^+	Sb_4^+
IPa (eV)	8.95	7.83	6.61
D (eV)	0.65	0.84	1.4

Figure Captions

Figure 1 The HeI photoelectron spectrum of P_4^+.

Figure 2 The HeI photoelectron spectrum of As_4^+.

Figure 3 The HeI photoelectron spectrum of Sb_4^+. The arrow indicates the $^2\Sigma_g^+$ band of Sb_2^+. Some contributions from Sb^+ atomic lines are subtracted. The $(2t_2)^{-1}$ bands have some contributions from the $^2\Pi_{u1/2}$ and $^2\Pi_{u3/2}$ bands of Sb_2^+.

Figure 4 The normal modes of vibrations for tetrahedral M_4 molecules. The x, y, and z axes lie along the three two-fold axes.

Figure 5 Diagram showing the adiabatic potential energy surfaces of the linear E⊗e Jahn-Teller Hamiltonian. $E(\rho,\phi)$ is plotted according to Eq. (2), for k = 5.75, a value deduced from spectral simulations to be that most appropriate for P_4^+. The floor of the potential lies at an energy of 16.5, in units of the zeroth-order harmonic frequency, below the conical intersection.

Figure 6 Correlation diagram showing the relative energies of the exact vibronic levels of the linear E⊗e Hamiltonian as a function of the distortion parameter, $D = 1/2k^2$. $|j| = 1/2$ harmonics of the radial oscillator are shown as solid lines. Other curves trace the $|j| > 1/2$ states of excited pseudorotation. In the linear limit, only transitions to states of the $|j| = 1/2$ block are allowed. Higher-order coupling mixes levels as j mod 3, altering the correlation diagram by avoided crossings and the spectrum by intensity sharing.

Figure 7 Linear Jahn-Teller fit to the vibronic profile of the $(1e)^{-1}$ band of the photoelectron spectrum of P_4^+. The linear coupling parameter, k, in units for which the harmonic force constant is 1, is 5.75. The progression of transitions to $j = 1/2$ radial harmonics originates at an adiabatic ionization energy of 8.95 eV. Positions and intensities were obtained at the converged

eigenvalues and eigenvectors of Eq. (5) for g = 0, diagonalized exactly in a basis of 800 two-dimensional harmonic oscillator wavefunctions.

Figure 8 Spectral simulations of P_4^+ spectrum constructed by convoluting theoretical positions and intensities (sticks), calculated for k = 5.75 and g from 0 to 0.1, with a 15 meV FWHM Gaussian instrumental function. Theoretical positions and intensities for g > 0 were obtained by diagonalizing Eq. (5) iteratively in a basis of 1302 isotropic two-dimensional harmonic oscillator wavefunctions using the Lanczos method.[32] (a) g = 0; (b) g = 0.005; (c) g = 0.008; (d) g = 0.01; (e) g = 0.02; (f) g = 0.05; (g) g = 0.1.

Figure 9 Diagram illustrating the adiabatic potential energy surfaces of the linear plus quadratic E⊗e Jahn-Teller Hamiltonian. $E(\rho,\phi)$ is plotted according to Eq. (17), for k = 5.75 and g = 0.02. The floor of the potential is modulated by three barriers that extend to a height of 0.66 in units of the zeroth-order harmonic frequency.

Figure 10 Linear Jahn-Teller fit to the $(1e)^{-1}$ band of the As_4^+ photoelectron spectrum. The linear coupling parameter, k, in units for which the harmonic force constant is 1, is 9.7. The progression of transitions to j = 1/2 radial harmonics originates at an adiabatic ionization energy of 7.83 eV. Positions and intensities were obtained as in Figure 7.

Figure 11 Linear Jahn-Teller fit to the $(1e)^{-1}$ band of the Sb_4^+ photoelectron spectrum. The linear coupling parameter, k, in units for which the harmonic force constant is 1, is 12.5. The progression of transitions to j = 1/2 radial harmonics originates at an adiabatic ionization energy of 6.61 eV. Positions and intensities were obtained as in Figure 7.

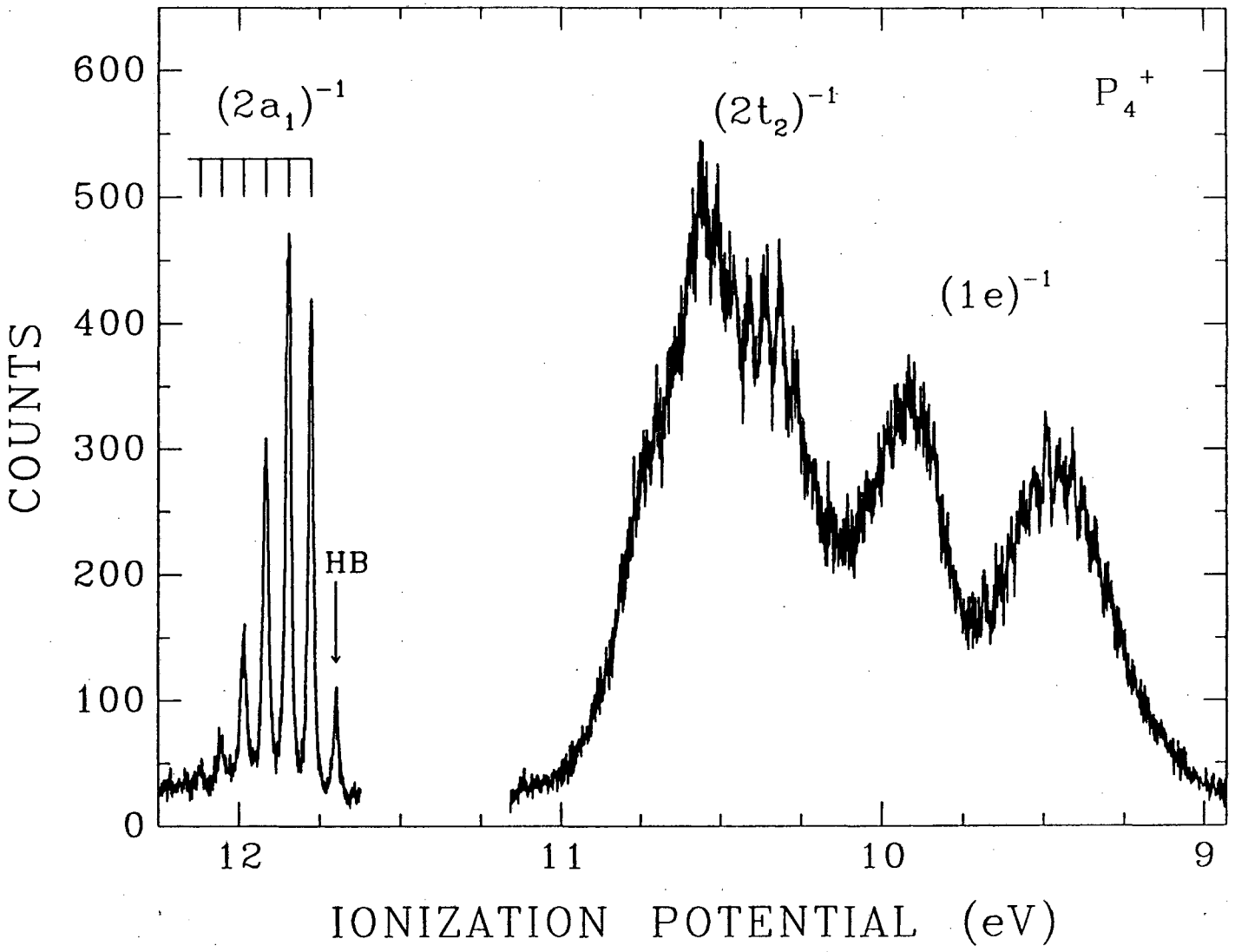

XBL 902-404

Figure 1

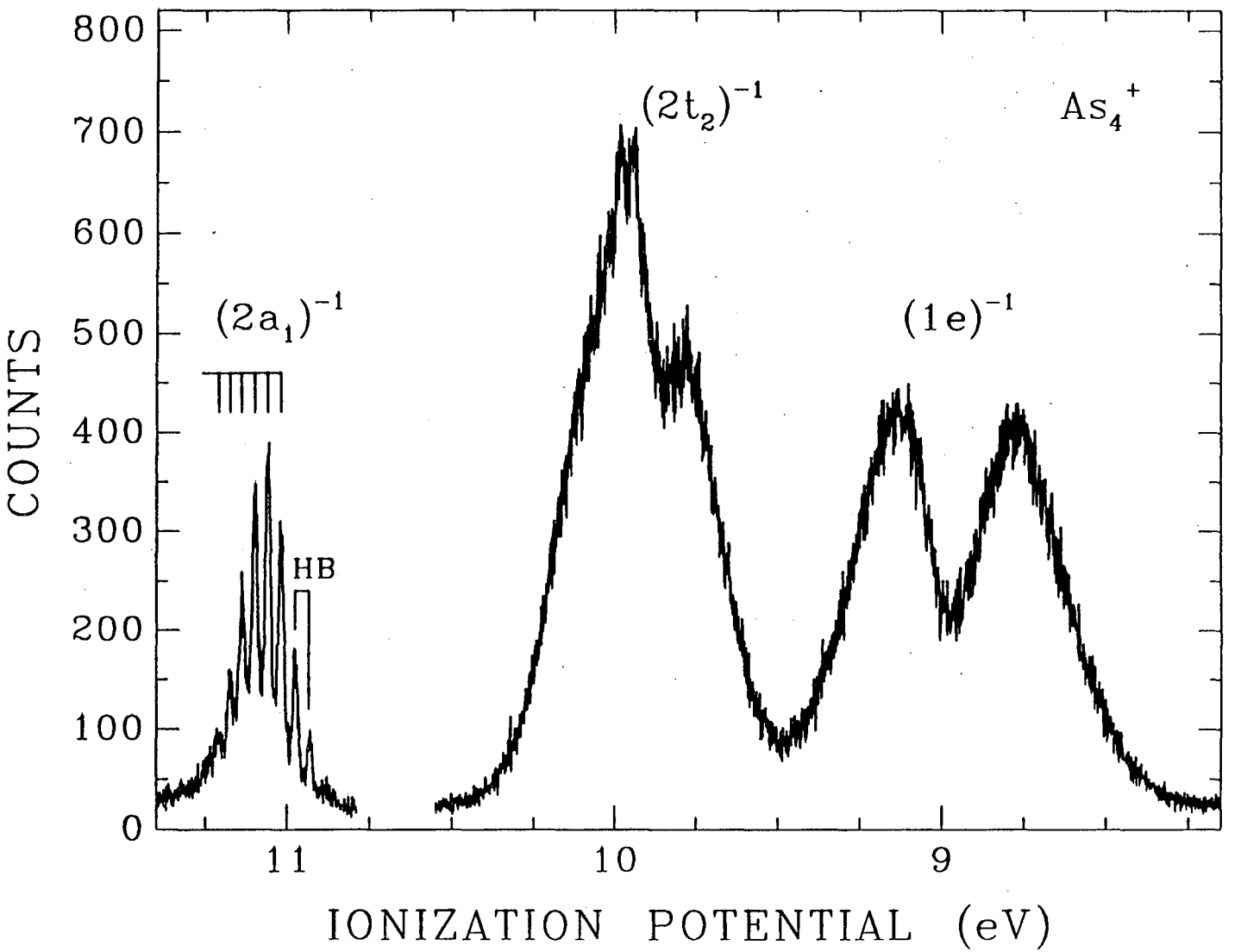

XBL 902-405

Figure 2

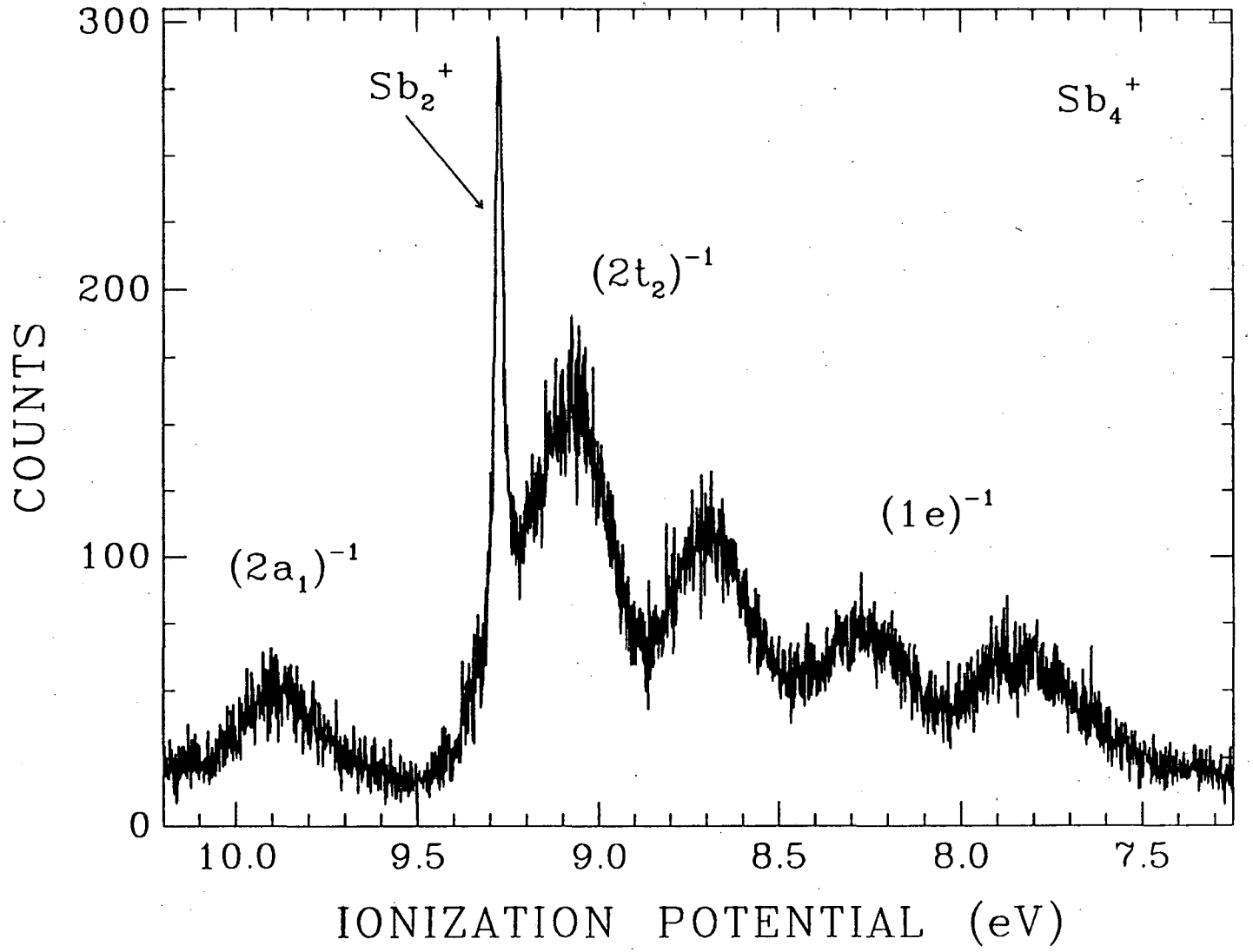

XBL 902-406

Figure 3

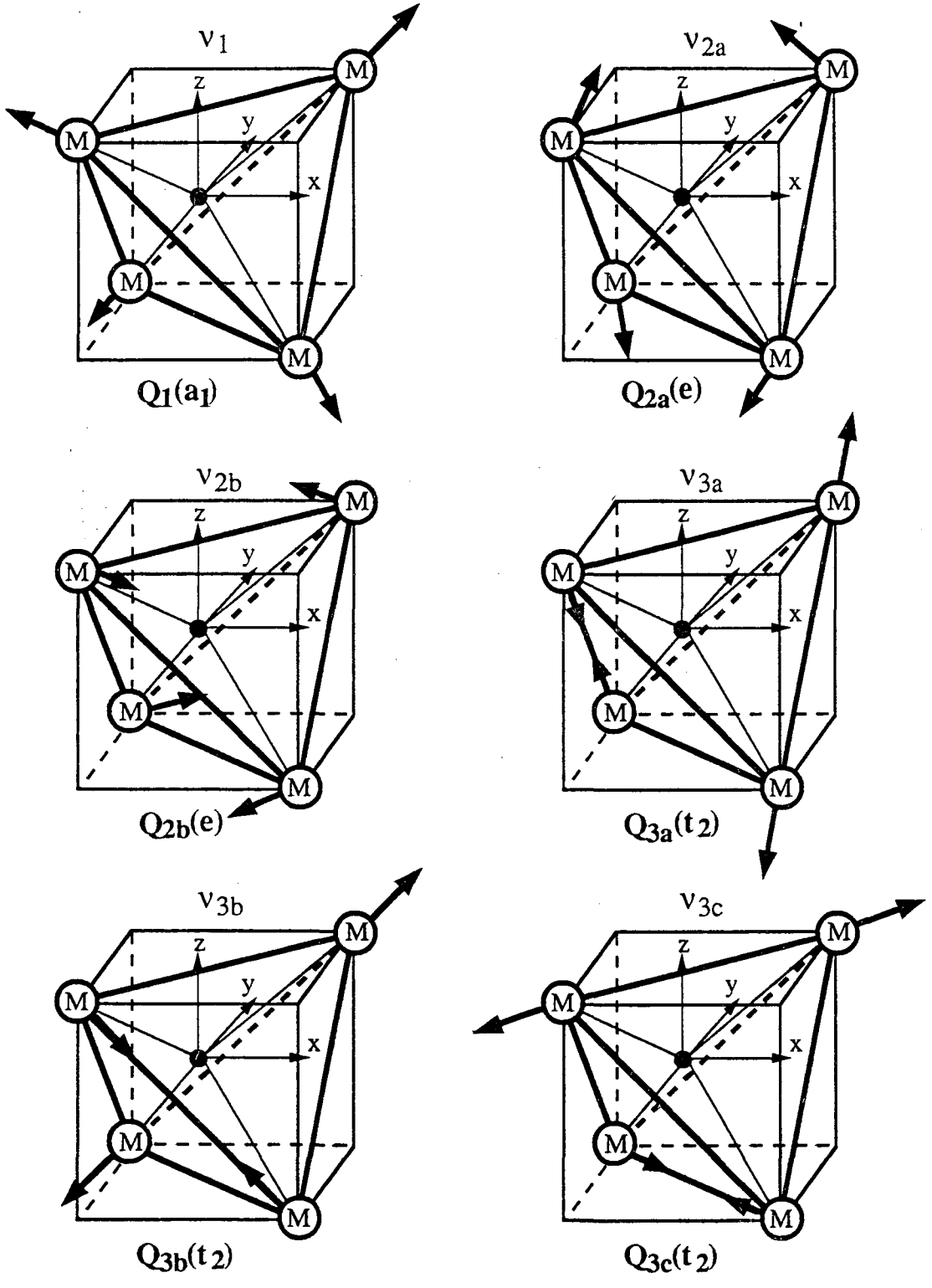

Figure 4

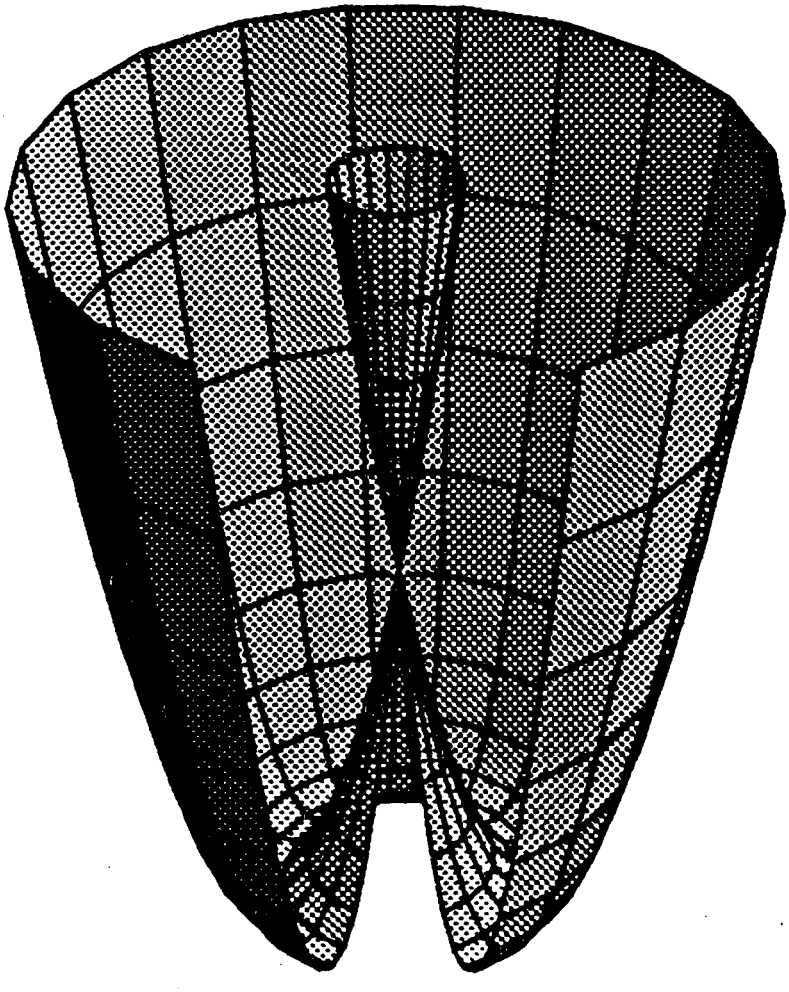

XBL 902-410

Figure 5

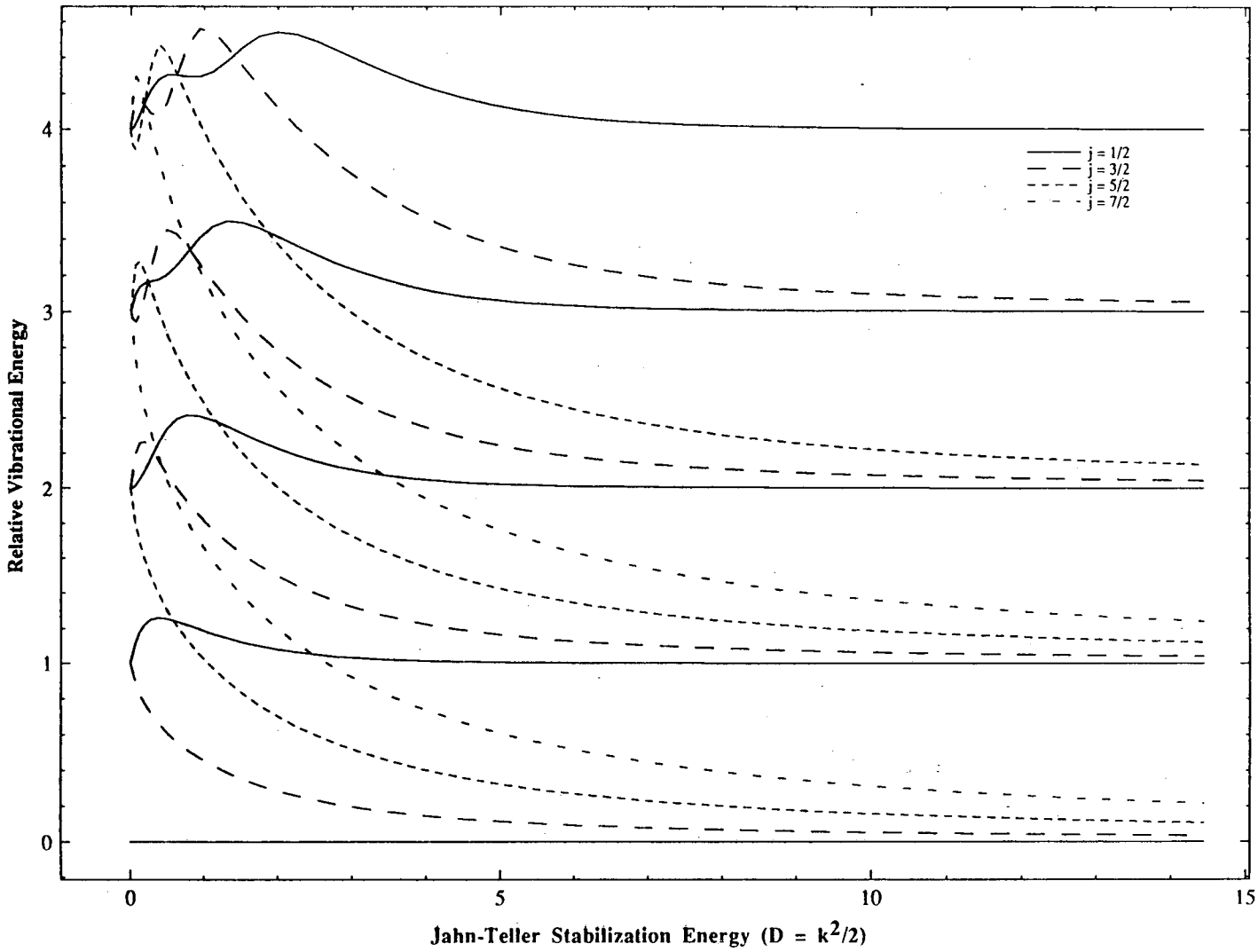

XBL 902-411

Figure 6

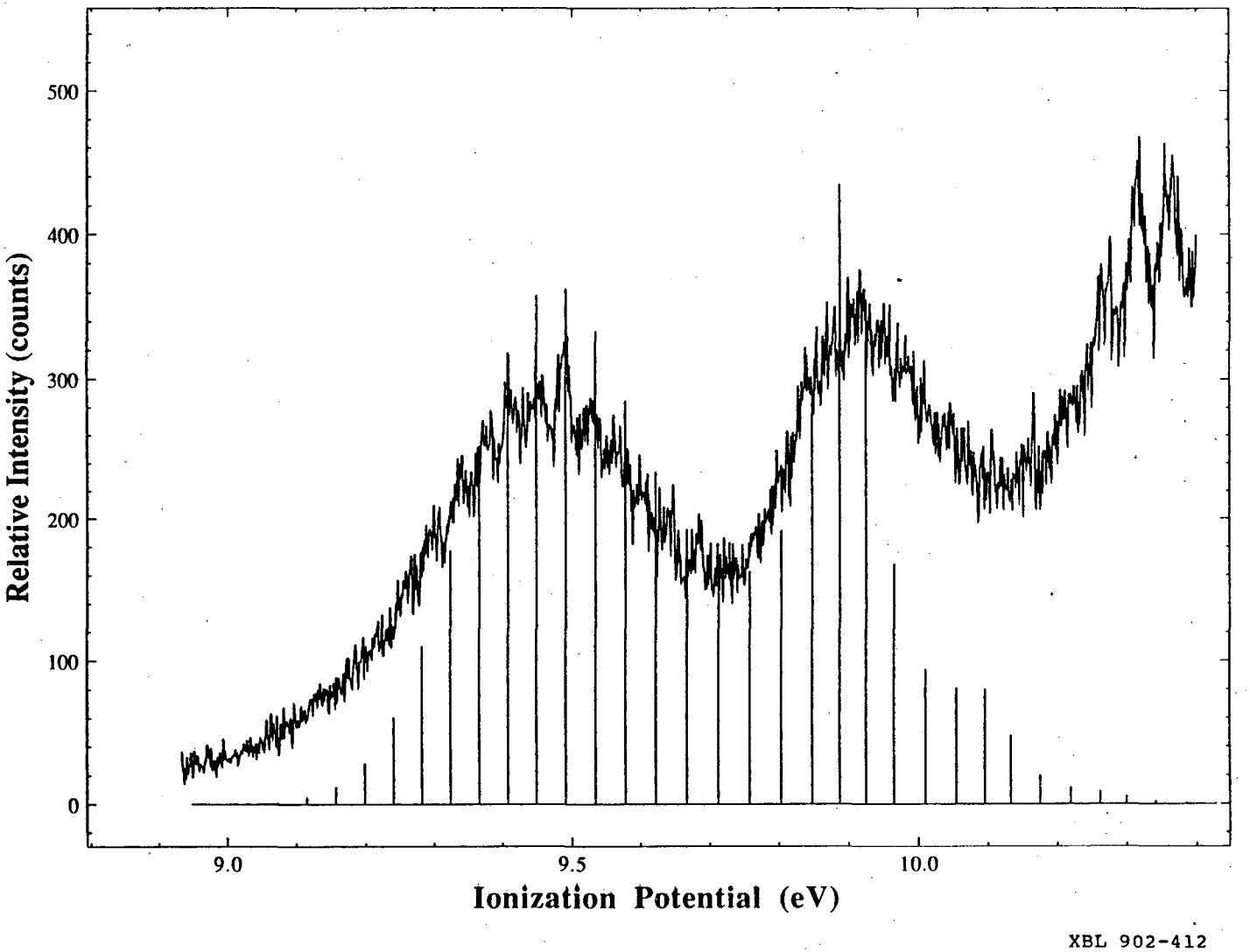
Relative Intensity (counts)
500
400
300
200
100
0
9.0
9.5
10.0
Ionization Potential (eV)
XBL 902-412

Figure 7

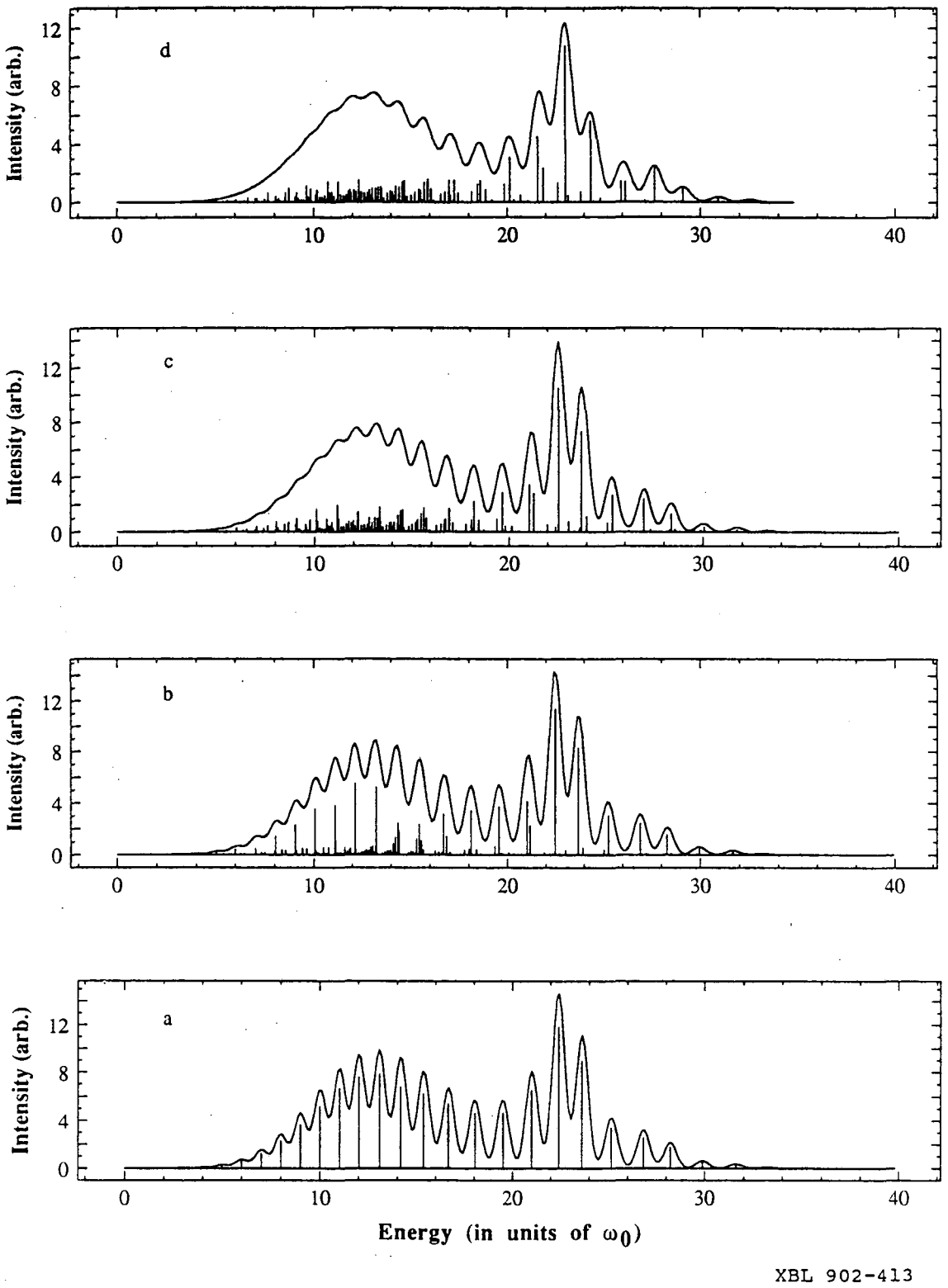
d
c
b
a
Intensity (arb.)
0
4
8
12
0
10
20
30
40
Energy (in units of ω_0)
XBL 902-413

Figure 8

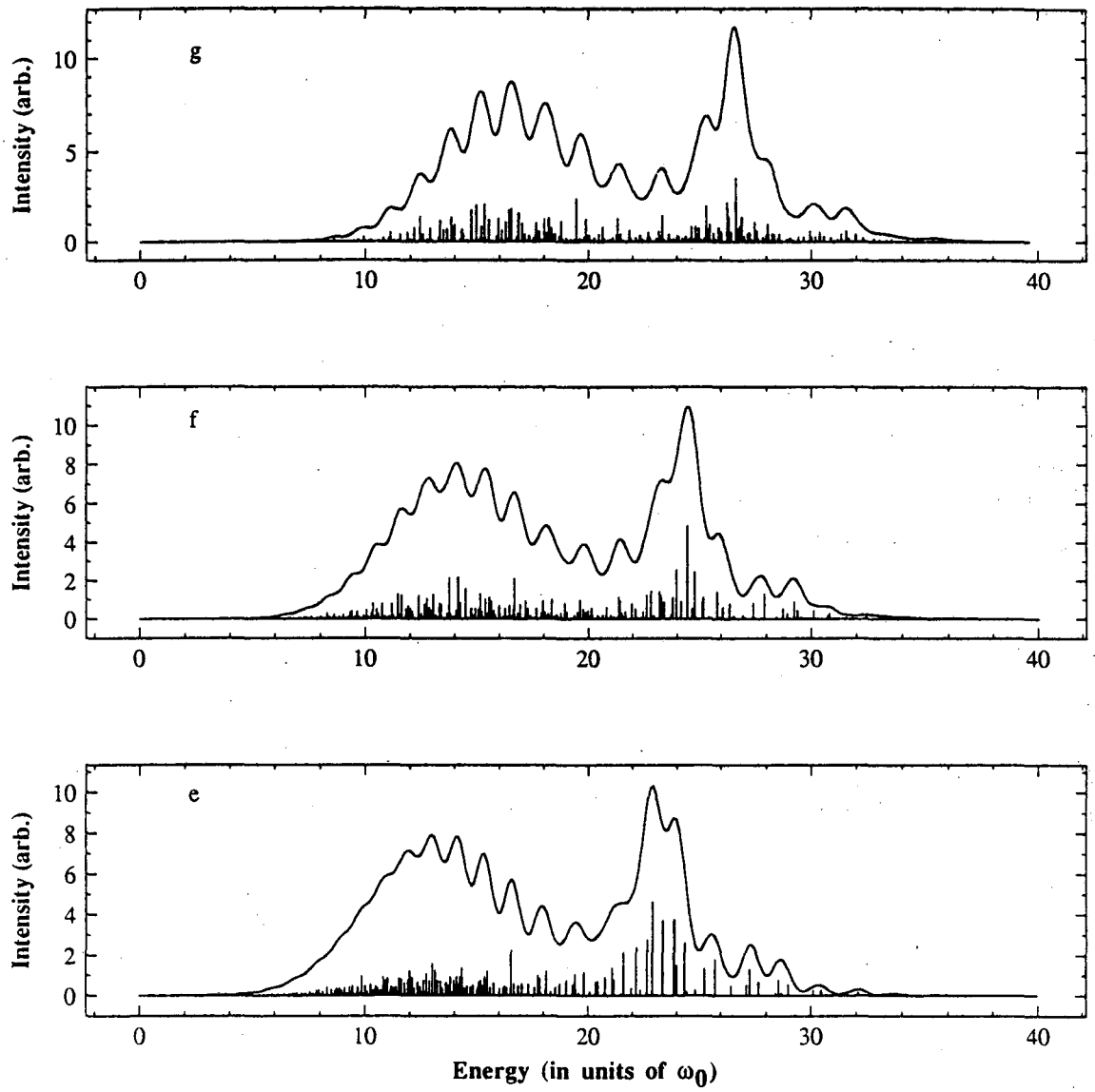

Figure 8 (Continued)

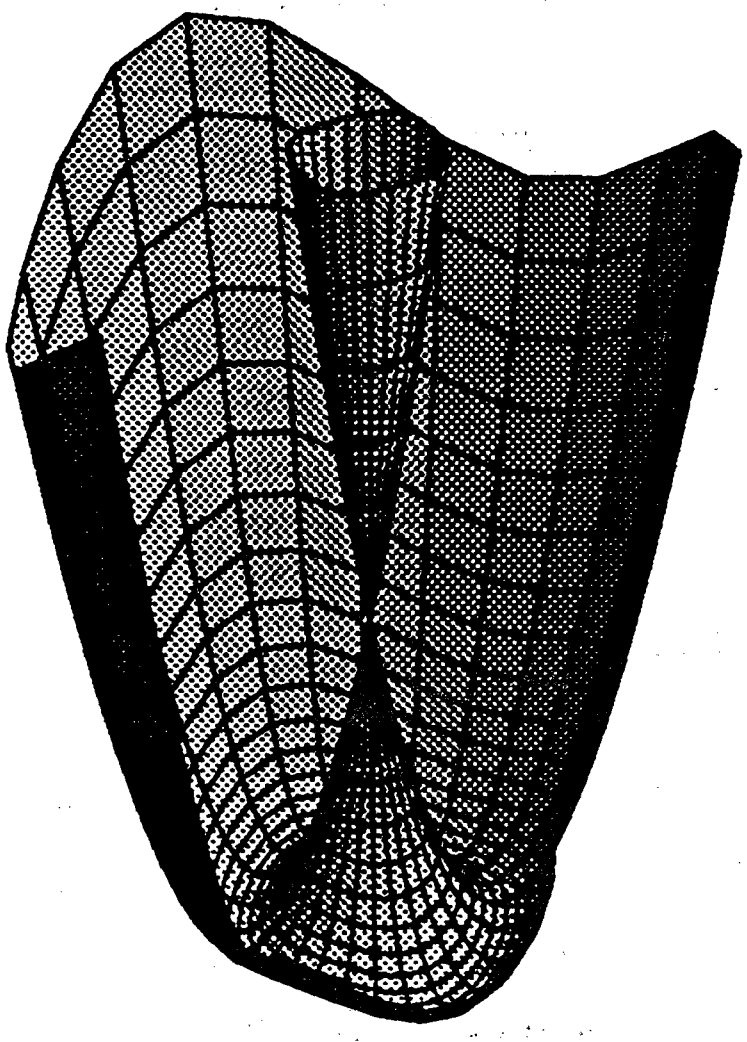

XBL 902-415

Figure 9

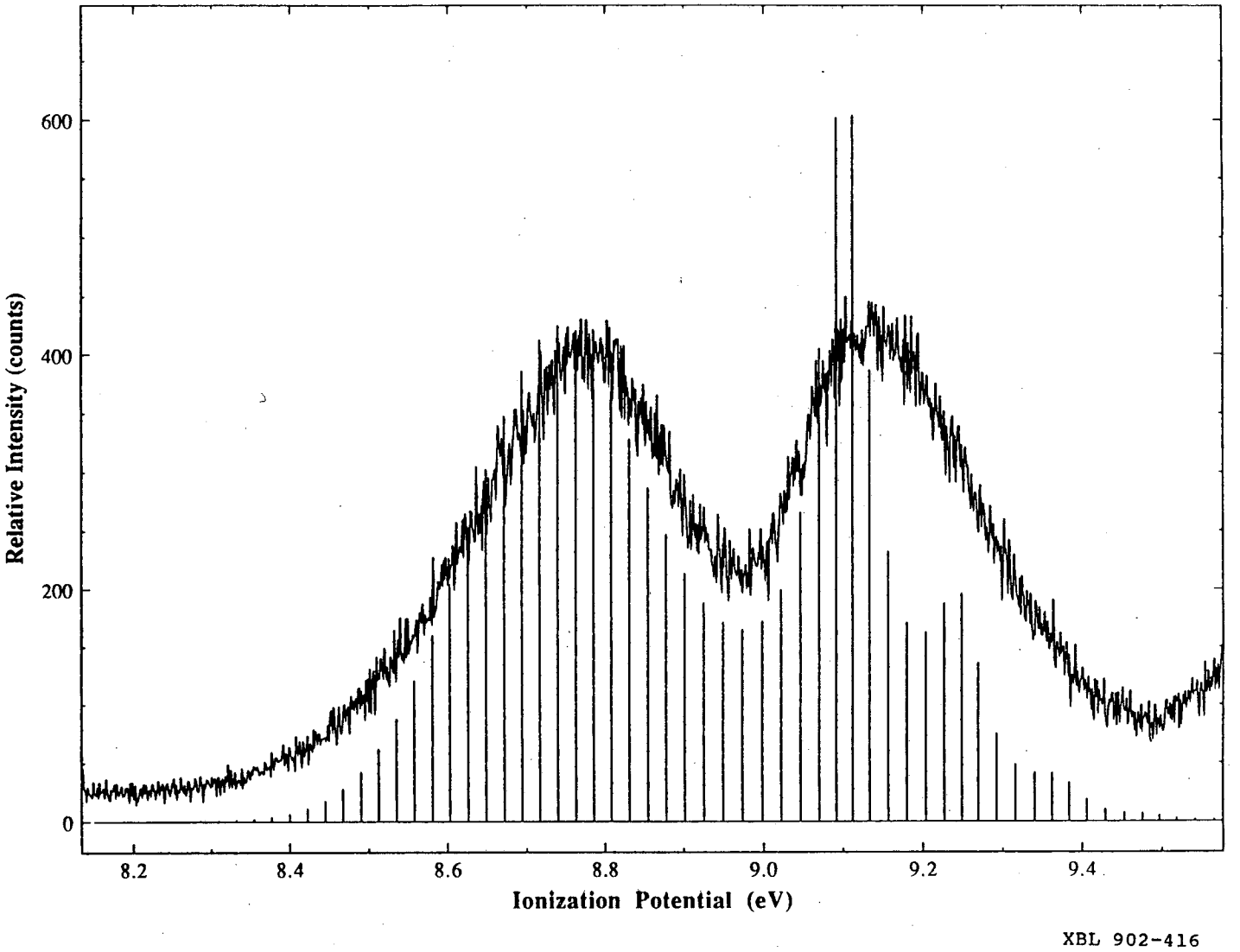
600
400
200
0
Relative Intensity (counts)
8.2
8.4
8.6
8.8
9.0
9.2
9.4
Ionization Potential (eV)
XBL 902-416

Figure 10

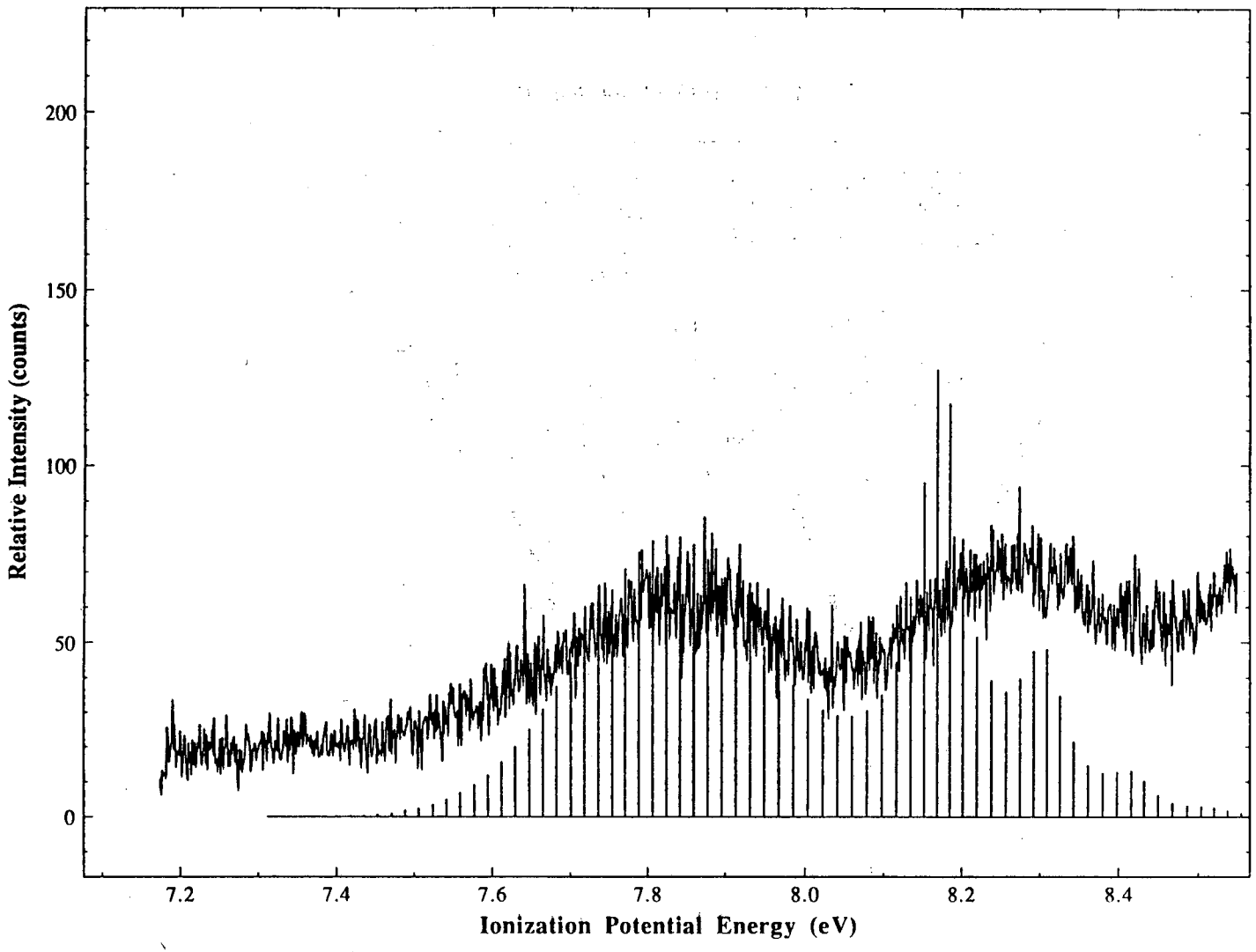

XBL 902-417

Figure 11

LAWRENCE BERKELEY LABORATORY
UNIVERSITY OF CALIFORNIA
INFORMATION RESOURCES DEPARTMENT
BERKELEY, CALIFORNIA 94720

LAWRENCE BERKELEY LABORATORY
UNIVERSITY OF CALIFORNIA
INFORMATION RESOURCES DEPARTMENT
BERKELEY, CALIFORNIA 94720